A Design of a 3rd Harmonic Cavity for the TTF 2 Photoinjector

J. Sekutowicz, R. Wanzenberg
DESY, Notkestr. 85, 22603 Hamburg, Germany

W.F.O. Müller, T. Weiland
TEMF, TU Darmstadt, Schloßgartenstr. 8, 64289 Darmstadt, Germany

July 18, 2002

Abstract

A design of a superconducting 3.9 GHz cavity for the injector of the TTF FEL-User Facility is presented. The cavity will be located after the first TESLA module with eight 1.3 GHz cavities and before the first bunch compressor. The purpose of the cavity is to cancel nonlinear distortions in the longitudinal phase space due to the cosine-like curvature of the 1.3 GHz accelerating cavity voltage. The basic cavity rf parameters and the properties of the higher order modes calculated with several computer codes are shown.

1 Introduction

It has been proposed in design studies for phase II of the TESLA test facility [1] to use a third harmonic (3.9 GHz) cavity to compensate nonlinear distortions of the longitudinal phase space due to cosine-like curvature of the cavity voltage of the 1.3 GHz TESLA cavities [2]. A schematic layout of the photoinjector and the first bunch compressor of the TESLA Test Facility II (TTF) is shown in Fig. 1. It is considered to generate relatively long bunches

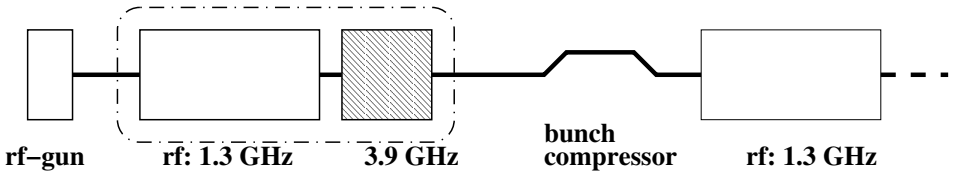

Figure 1: Schematic layout of the TTF2 Test Facility.

($\sim$ 2 mm rms) with the rf-gun to mitigate space charge effects and their impact on the transverse emittance. The long bunches are accelerated to an energy of about 180 MeV using a TESLA module with eight 1.3 GHz accelerating cavities and are subsequently longitudinally compressed in a four dipole achromatic chicane. In Ref. [1] it is shown how the incoming beam is longitudinally "matched" to the bunch compressor using the 1.3 GHz and 3.9 GHz rf-systems. As indicated in Fig. 1 the 3.9 GHz cavities may be integrated in an extended module together with the 1.3 GHz cavities.

A certain energy spread $\delta(s) \approx -s/R_{56}$ along the bunch (longitudinal coordinate s, $R_{56} = \partial s/\partial\delta$ first order matrix element of the bunch compressor in TRANSPORT [3] notation) is required to compress the bunches. But for a basic understanding of the parameter dependencies of the two rf-systems it is sufficient to consider the situation where the goal is to compensate the energy spread within a bunch which is accelerated on crest of the 1.3 GHz rf-system voltage. The sum of the accelerating voltages of the two rf-systems is

$$V(s) = V_0 \cos(\omega_0\, s/c) + V_1 \cos(\omega_1\, s/c + \phi_1), \tag{1}$$

where V_0 is the amplitude of the $\omega_0 = 2\,\pi \cdot 1.3\,\mathrm{GHz}$ rf-system and V_1 the amplitude of the second rf-system, which is operated at the frequency ω_1 with the relative rf-phase ϕ_1 with respect to the first system.

Using the Taylor expansion at $s = 0$ of the sine and cosine functions, $\sin(\omega_1\, s/c) \approx \omega_1\, s/c$ and $\cos(\omega_{0,1}\, s/c) \approx 1 - 1/2\,(\omega_{0,1}\, s/c)^2$, one can rewrite Eqn. (1) as

$$\begin{aligned} V(s) &= V_0 \cos(\omega_0\, s/c) + \\ &\quad V_1 \cos(\phi_1) \cos(\omega_1\, s/c) - V_1 \sin(\phi_1) \sin(\omega_1\, s/c) \\ &\approx V_0 + V_1 \cos(\phi_1) \\ &\quad -V_1\, \omega_1\, (s/c) \sin(\phi_1) \\ &\quad -\frac{1}{2}\,(\omega_0\, s/c)^2 \left(V_0 + V_1\, (\frac{\omega_1}{\omega_0})^2 \cos(\phi_1) \right) \end{aligned} \tag{2}$$

The voltage is approximately constant within the bunch if the following conditions are fulfilled:

a) $\phi_1 = -180^\circ$ to cancel the term proportional to s/c and

b) $V_1 = \frac{-1}{\cos(\phi_1)} (\frac{\omega_0}{\omega_1})^2 V_0$ to cancel the term quadratic in s/c.

Under these conditions the sum of the cavity voltages is constant (up-to second order):

$$V(s) \approx V_0 \left(1 - (\frac{\omega_0}{\omega_1})^2\right) = \text{const.} \tag{3}$$

It is important to note that it is the frequency ratio which determines the amplitude V_1 of the second rf-system (condition **b)**). As an example consider 8 TESLA cavities operated at a gradient of 22 MV/m and a 3rd harmonic second rf-system. The required amplitude of the second system is: $V_1 = V_0/9 = 19.5\,\text{MV}$, with $V_0 = 8\,\text{m} \times 22\,\text{MV/m} = 176\,\text{MV}$.

Furthermore it is required to operate both systems in a **multibunch mode**. The rf-frequency ω_1 has to be chosen such that

$$\begin{aligned} V(s) &= V(s + c\,\Delta t) \\ &= V(s + c\,n_{FB}\frac{2\pi}{\omega_0}), \end{aligned} \tag{4}$$

where Δt is the bunch spacing, which may be also expressed in terms of n_{FB}, the number of free 1.3 GHz buckets between bunches. Typical bunch spacings are:

$1/\Delta t$	n_{FB}	
1 MHz	1300	$= 2^2 \cdot 5^2 \cdot 13$
10 MHz	130	$= 2 \cdot 5 \cdot 13$

The condition of Eqn. (4) is fulfilled, if

$$n_{FB}\,\frac{\omega_1}{\omega_0} = \text{integer}. \tag{5}$$

The choice $\frac{\omega_1}{\omega_0} = \text{integer}$ fulfills the condition (5) for all bunch distances n_{FB}. But $\frac{\omega_1}{\omega_0} = 2.3$ or $\omega_1 = 2\pi \cdot 2.99\,\text{GHz}$ (S-Band) is also a reasonable possibility for a second rf-system, since

$$n_{FB}\,\frac{\omega_1}{\omega_0} = 130 \cdot 2.3 = 299,$$

is an integer. Any bunch distance n_{FB} which is a multiple of 130 is also a possible multibunch operation mode with an second S-band rf-system. But a higher amplitude of $V_1 = V_0/5.29 = 33.3\,\text{MV}$ for the second rf-system is required for this choice for ω_1.

The relative voltage $V(s)/V(0)$ is shown in Fig. 2 for both cases $\omega_1/\omega_0 = 3$ (3rd harmonic) and $\omega_1/\omega_0 = 2.3$ (S-band). In both cases one obtains a constant voltage within the bunch over a range of ± 2 mm and only small nonlinear deviations within a range of about ± 5 mm. The nonlinear distortion

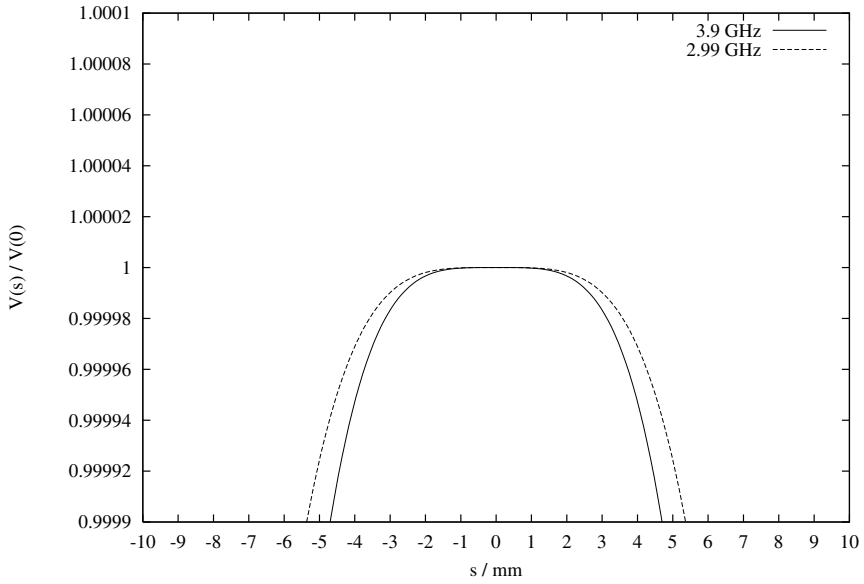

Figure 2: Sum of the cavity voltages as a function of the position in the bunch normalized with respect to the voltage in the bunch center. Wakefields are not included in this plot.

of the voltage due to wakefields [4] has not been included in the calculations. Since the required amplitude V_1 is smaller for a 3rd harmonic rf-system we will consider the design of a 3.9 GHz cavity. The cell dimensions of a TESLA cavity [2] and a TESLA cavity scaled to a frequency of 3.9 GHz are summarized in table 1. An iris radius of the end-cells of 13 mm is too small to mount a coaxial high power coupler at the beam pipe. Therefore a new cavity shape has been designed which is presented in the next section.

	midcup		end-cup 1		end-cup 2	
iris radius a /mm	35.0	(11.67)	39.0	(13.0)	39.0	(13.0)
equator radius b /mm	103.3	(34.43)	103.3	(34.43)	103.3	(34.43)
half cell length h /mm	57.7	(19.23)	56.0	(18.67)	57.0	(19.0)
curvature at equator r_e/mm (circle) ($r_e = r_{ez} = r_{er}$)	42.0	(14.0)	40.3	(13.4)	42.0	(14.0)
iris - horz. axis r_{iz}/mm	12.0	(4.0)	10.0	(3.33)	9.0	(3.0)
- vert. axis r_{ir}/mm	19.0	(6.33)	13.5	(4.5)	12.8	(4.27)

Table 1: Geometric parameters of three cup shapes of a TESLA 1.3 GHz cavity and (in brackets) of a TESLA cavity scaled to 3.9 GHz.

2 Design of a 3.9 GHz Cavity

A two dimensional (2D) Frequency Domain Finite Element Method (FD FEM) code [5] has been used by J. Sekutowicz to design a 3.9 GHz 9-cell cavity with an iris diameter of 30 mm. The FD-FEM code uses a mesh with both straight and curvilinear triangles to obtain a very accurate approximation of the cavity geometry. The absolute value of the electric field of the π-mode is shown in Fig. 3.

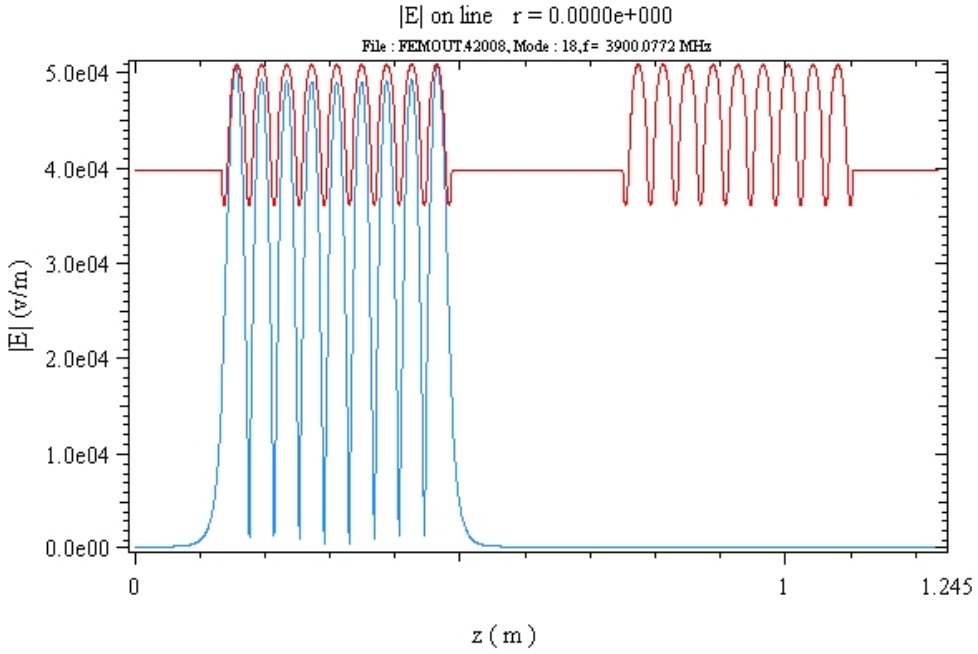

Figure 3: Two 9-cell cavities modeled with a FD-FEM code. The absolute value of the electric field of the π-mode is shown.

2.1 Geometry

One 3.9 GHz cavity consists of nine cells with a elliptical cup shape. The end-cups have a slightly different shape to obtain a good field-flatness of the π-mode. At the end of the cavities there is a transition from the cavity iris (with a diameter of 30 mm) to the beam pipe with a diameter of 80 mm which is needed to mount a coaxial input coupler of approximately the same diameter at the beam pipe near an end-cell. A sketch of a cavity half cell is given in Fig. 4. A complete list of the cavity cell parameters are given in table 2.

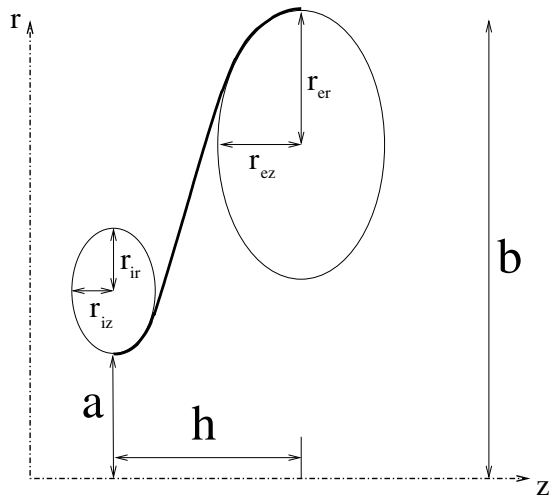

Figure 4: Schematic sketch of the cavity geometry.

	mid-cup	end-cup
iris radius a /mm	15.0	15.0
equator radius b /mm	35.787	35.787
half cell length h /mm	19.2167	19.2167
curvature at		
equator - horz. axis r_{ez}/mm	13.6	13.6
- vert. axis r_{er}/mm	15.0	15.0
iris - horz. axis r_{iz}/mm	4.5	4.5
- vert. axis r_{ir}/mm	6.0	6.0

Table 2: Geometric parameters of the mid-cup and end-cups of a 3.9 GHz cavity.

2.2 Basic rf-parameters

3rd harmonic cavity design parameters:		
Type of accelerating structure	standing wave	
Accelerating mode	π-mode	
Frequency	3900	MHz
Active length	0.3459	m
Number of cells	9	
R/Q	391	Ω
Geometry factor (G_1)	273	Ω
Nominal accelerating gradient	20	MV/m
Stored energy (20 MV/m)	2.5	J
E_{peak}/E_{acc}	2.26	
B_{peak} (20 MV/m)	0.097	T

Table 3: Basic RF-design parameter of the 3rd harmonic cavity.

The FD-FEM code has been used to compute the basic rf-parameters of the accelerating mode and some higher monopole modes. The parameters

for the the 3.9 GHz accelerating mode are summarized in table 3.

The following convention has been used to compute the characteristic value R/Q:

$$\frac{R}{Q} = \frac{|V_z(r)|^2}{2\,\omega\,U},$$

where U is the total stored energy in the mode, $\omega = 2\pi\,f$ and $V_z(r)$ is the voltage

$$V_z(r) = \int_0^L dz\, E_z(r,z) \exp(-i\,\omega\,z/c)$$

at the radial position r. R/Q is independent of the radial position r for all monopole modes. The integration is performed on the axis ($r = 0$) of the cavity. The power dissipated into the cavity wall is characterized by the quality factor Q_0 or the geometry parameter G_1:

$$Q_0 = \frac{\omega\ U}{P_{sur}}, \qquad\qquad G_1 = R_{sur}\ Q_0,$$

where P_{sur} is the power dissipated into the cavity wall due to the surface resistivity R_{sur}.

The parameters of 50 monopole modes have been calculated for two 9-cell cavities. The results can be found in tables 4 and 5. For all modes with a

Two 9-cell cavities monopole modes:

f / MHz	R/Q / Ω	G_1 / Ω	Q_{Cu}
3745.594482	0.0015	270.4	16936
3745.595215	0.0015	270.4	16936
3758.746826	0.0060	270.6	16919
3758.747070	0.0060	270.6	16919
3779.136475	0.0095	270.9	16893
3779.136963	0.0095	270.9	16893
3804.557861	0.0275	271.3	16859
3804.557861	0.0275	271.3	16859
3832.135498	0.0150	271.7	16821
3832.135498	0.0150	271.7	16821
3858.571289	0.0625	272.0	16783
3858.571289	0.0625	272.0	16783
3880.517822	0.0240	272.2	16750
3880.517822	0.0240	272.2	16750
3895.043457	0.0930	272.4	16727
3895.043701	0.0930	272.4	16727
3900.076904	391.1720	273.0	16753
3900.077148	391.1710	273.0	16753

Table 4: RF-parameters of 50 monopole modes of two 9-cell cavities computed with the FD-FEM code (part 1).

frequency below the cutoff frequency of the beam pipe are there always two modes with almost identical frequencies corresponding to a mode with field

f / MHz	R/Q / Ω	G_1 / Ω	Q_{Cu}
5758.775879	9.5730	453.5	22908
5758.776367	0.0115	453.5	22908
5758.776367	9.5645	453.6	22908
5823.605469	0.1490	455.5	22879
5931.120605	7.0550	459.5	22869
5931.121582	0.2640	459.5	22869
5931.122559	7.0465	459.5	22869
6080.165527	0.0335	466.2	22915
6268.597168	7.5970	476.0	23043
6268.599121	0.5820	476.0	23043
6268.600586	7.5905	476.0	23043
6492.987793	0.3185	489.0	23261
6747.714355	9.8485	504.9	23557
6747.715332	0.0045	504.9	23558
6747.716309	9.8325	504.9	23558
7017.748535	0.1365	515.6	23592
7039.958008	0.0035	462.6	21133
7040.976074	0.0005	464.6	21223
7072.179199	0.0000	463.5	21124
7074.048828	0.0075	464.8	21180
7122.615723	0.1070	465.6	21147
7125.318848	0.0155	466.0	21161
7185.799316	0.0145	470.9	21290
7190.372559	0.2980	470.2	21255
7248.857910	0.3655	489.0	22016
7258.693359	0.2090	485.7	21852
7306.385254	5.9160	502.4	22526
7323.582520	0.6050	507.0	22709
7372.916016	2.3055	490.2	21883
7395.319336	8.0855	481.2	21445
7469.971680	30.1965	501.7	22248

Table 5: RF-parameters of 50 monopole modes of two 9-cell cavities computed with the FD-FEM code (part 2).

in one or the other of the 9-cell cavities, like the mode shown in Fig. 3. Modes from higher passbands can propagate into the beam pipe and may have field components in both 9-cell cavities as well in the beam pipe between the two 9-cell cavities.

3 Higher order dipole modes

The long range wakes due to Higher Order Modes (HOMs) can cause energy deviations and kicks on the bunches, which can result in orbit deviations within the bunch train or in the worst case in a cumulative beam-breakup instability. To provide the data needed for tracking studies the computer codes MAFIA [6, 7] and MICROWAVE Studio (MWS) [8] have been used to compute the dipole modes in a 9-cell cavity up to a frequency of about 10 GHz. The long range dipole wake potential [4] is a sum over all dipole modes:

$$W_{\perp}^{(1)}(s) = c \sum_n \left(\frac{R^{(1)}}{Q}\right)_n \sin(\omega_n\, s/c)\ \exp(-1/\tau_n\ s/c),$$

where $(R^{(1)}/Q)_n$ is the R/Q-value of the n-th dipole mode, measured in Ω/cm^2, $\omega_n = 2\pi\, f_n$ is the frequency and τ_n is the damping time of the mode n. For superconducting cavities the damping time τ_n is usually dominated by the external Q-value:

$$\tau_n \approx \frac{2\,(Q_{ext})_n}{\omega_n},$$

which depends on the success of HOM-couplers used to damp these modes. The design of HOM-couplers is beyond the scope of these report, which only presents results on the frequencies, R/Q-values and geometric factors to provide a basis for further investigations.

3.1 Dipole passbands

The dipole mode passband structure of a cavity mid-cell has been calculated using the MAFIA eigenvalue solver with periodic boundary conditions:

$$\boldsymbol{E}(r, z+g) = \boldsymbol{E}(r, z)\ \exp(i\varphi),$$

where φ is the phase advance per cell, and g the cell length. The phase advance per cell is used as an abscissa in the plot of the dipole passbands in Fig. 5.

A beam excites most strongly those modes which are synchronous to the beam, i.e. modes with a phase velocity equal to the speed of light:

$$c = v_{ph} = \frac{\omega}{k_z} = 2\,\pi\ g\ \frac{f}{\varphi}, \tag{6}$$

where k_z is the longitudinal wave number (sometimes also denoted as β) and which is used as an abscissa in the plots of the dispersion curves. The light cone is the straight line $f(\varphi) = \varphi\, c/(2\,\pi\, g)$, which is folded into the phase range from 0 to 180° in Fig. 5 using the periodicity of the structure. The 0-mode and the π-mode frequencies of the 5th passband differ by only 80 MHz, indicating that the cell-to-cell coupling is weak and that there might be nearly trapped modes in a 9-cell cavity. But the passbands of a periodic structure provide only first hints on the dipole modes in cavities with a finite number of cells. It is still necessary to investigate the modes in a 9-cell structure in more detail.

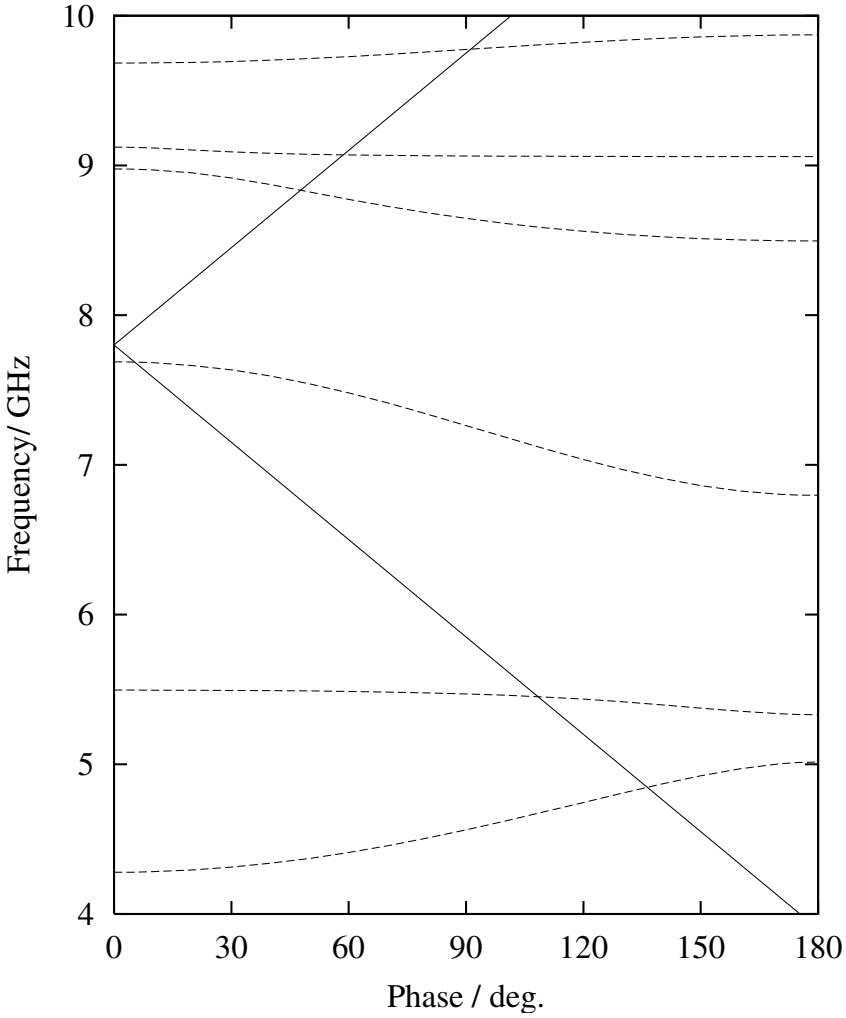

Figure 5: Dipole mode passbands of a cavity mid-cell.

3.2 Dipole modes in a 9-cell cavity

The electric field of the first 4 dipole modes are shown in Fig. 6 to Fig. 9. The 4-th mode can already propagate into the beam pipe since the cut-off frequency of the lowest dipole TE-mode is 4.3925 GHz. The R/Q parameter of most of the dipole modes will therefore depend on the length of beam pipe between the 9-cell cavities. For the MAFIA calculation a total cavity length of 64.69 cm is used. The active cavity length of the 9-cell cavity is 34.59 cm. The additional space is necessary for the input and HOM-couplers. The

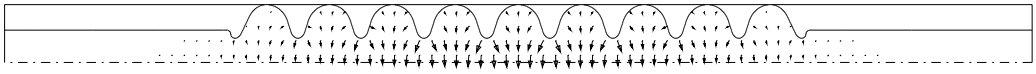

Figure 6: Electric field of the dipole mode EE-1 (MAFIA calculation).

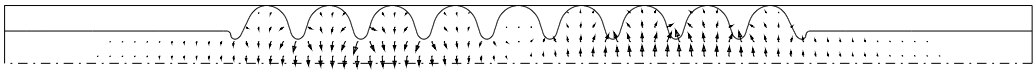

Figure 7: Electric field of the dipole mode EE-2 (MAFIA calculation).

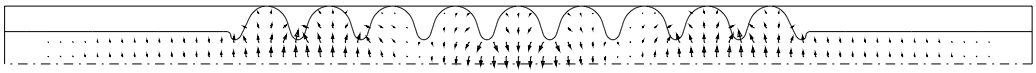

Figure 8: Electric field of the dipole mode EE-3 (MAFIA calculation).

Figure 9: Electric field of the dipole mode EE-4 (MAFIA calculation).

details of the cavity geometry used in the MAFIA calculations is shown in Fig. 10. The length of the beam pipe is 14.05 cm. The transition from the cavity iris radius of 15 mm to the beam pipe radius of 20 mm is included into the section of the pipe of length 14.05 cm, as indicated in Fig. 10. Since most

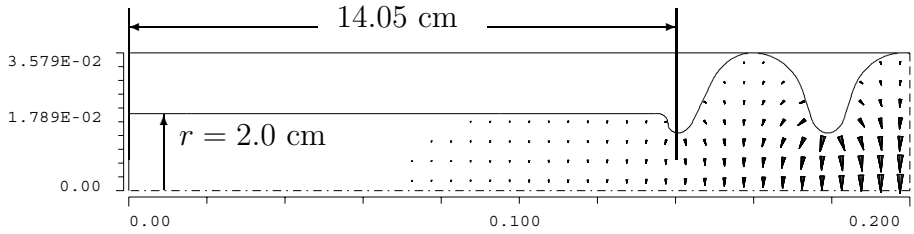

Figure 10: Electric field of the dipole mode EE-1 (MAFIA calculation). Enlarged view of the beam pipe and the first cavity cells of Fig.6.

of the dipole modes propagate into the beam pipe the value for R/Q depends on the length of the beam pipe and on the boundary conditions. Electric

($E_z = 0$) and magnetic ($B_z = 0$) boundary conditions have been used for the MAFIA calculations. A regular mesh with a mesh size of 0.2 mm was used for the discretization of the cavity geometry. A list of all considered modes is given in Tables 6 and 7. In total 140 modes have been considered. Large values for R/Q (above $1\,\Omega/\mathrm{cm}^2$) are printed in bold face. The electric field of several modes above the cutoff frequency of the beam pipe with a large R/Q are shown in Fig. 11 to 17.

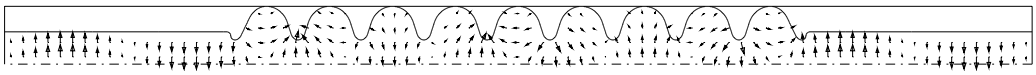

Figure 11: Electric field of the dipole mode EE-10 (MAFIA calculation).

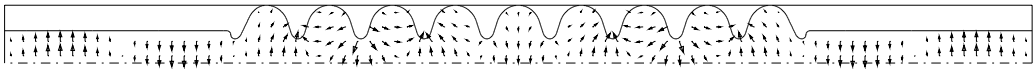

Figure 12: Electric field of the dipole mode EE-11 (MAFIA calculation).

Figure 13: Electric field of the dipole mode EE-19 (MAFIA calculation).

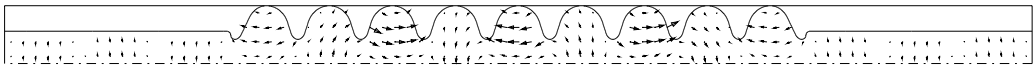

Figure 14: Electric field of the dipole mode EE-20 (MAFIA calculation).

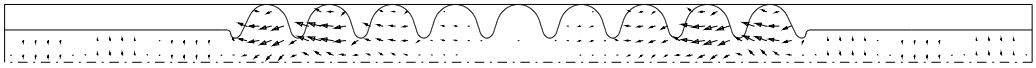

Figure 15: Electric field of the dipole mode EE-23 (MAFIA calculation)

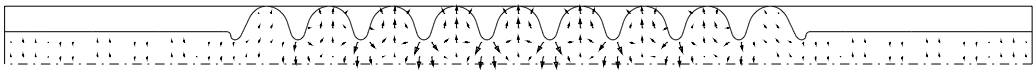

Figure 16: Electric field of the dipole mode EE-38 (MAFIA calculation).

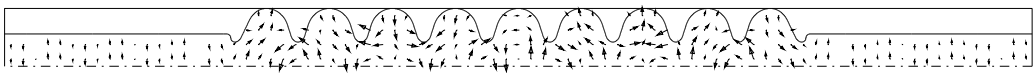

Figure 17: Electric field of the dipole mode EE-48 (MAFIA calculation).

mode	f / GHz	R/Q / Ω/cm^2	G_1 /Ω	mode	f / GHz	R/Q / Ω/cm^2	G_1 /Ω
EE- 1	4.2911	0.0053	232.9	MM- 1	4.2911	0.0053	232.9
EE- 2	4.3278	0.0338	237.0	MM- 2	4.3277	0.0343	237.0
EE- 3	4.3850	0.0959	243.0	MM- 3	4.3831	0.0735	242.6
EE- 4	4.4512	0.1413	249.0	MM- 4	4.4157	0.0596	246.4
EE- 5	4.4922	0.0000	253.3	MM- 5	4.4232	0.0635	248.2
EE- 6	4.5179	0.2182	258.3	MM- 6	4.4683	0.0277	252.7
EE- 7	4.5783	**1.1490**	265.0	MM- 7	4.5471	0.6554	259.3
EE- 8	4.6680	0.2361	271.2	MM- 8	4.6120	0.6350	265.3
EE- 9	4.7552	**13.2378**	275.0	MM- 9	4.6567	0.0061	272.9
EE-10	4.8220	**31.9650**	278.9	MM-10	4.7169	**6.1772**	280.4
EE-11	4.8797	**33.6595**	283.9	MM-11	4.8065	**37.6291**	284.3
EE-12	4.9522	**12.7711**	280.6	MM-12	4.9018	**44.9945**	283.3
EE-13	5.0561	0.0004	300.8	MM-13	4.9773	**8.0710**	277.2
EE-14	5.0678	**12.4796**	284.1	MM-14	5.0104	**3.1643**	262.6
EE-15	5.3551	0.0648	521.6	MM-15	5.1993	**2.4742**	368.2
EE-16	5.3976	**3.8163**	460.1	MM-16	5.2012	**2.4102**	361.5
EE-17	5.4267	**3.7699**	419.1	MM-17	5.3583	0.1900	511.5
EE-18	5.4402	**4.1318**	400.1	MM-18	5.4056	**5.6064**	453.3
EE-19	5.4551	**21.3217**	401.1	MM-19	5.4444	**23.8903**	424.2
EE-20	5.4737	**10.4197**	400.1	MM-20	5.4702	**13.6416**	407.6
EE-21	5.4867	0.0065	394.1	MM-21	5.4853	0.1614	397.3
EE-22	5.4933	0.5394	389.2	MM-22	5.4929	0.6536	390.5
EE-23	5.5027	**4.1888**	390.4	MM-23	5.5000	0.0536	393.6
EE-24	5.5027	0.0482	390.5	MM-24	5.5001	**2.7383**	393.3
EE-25	6.0286	0.3334	467.9	MM-25	5.7236	0.6329	448.5
EE-26	6.0286	0.0266	467.9	MM-26	5.7236	0.8758	448.5
EE-27	6.6464	0.0148	540.9	MM-27	6.3426	0.1631	538.5
EE-28	6.6467	0.4492	540.7	MM-28	6.3426	0.1226	538.5
EE-29	6.8306	0.0007	613.9	MM-29	6.8185	0.0136	613.6
EE-30	6.9180	0.0000	618.1	MM-30	6.8693	0.1734	613.4
EE-31	7.0324	0.0430	618.6	MM-31	6.9238	0.1714	612.1
EE-32	7.1491	0.0300	610.5	MM-32	6.9934	0.0975	616.2
EE-33	7.2519	0.0372	598.2	MM-33	7.0985	0.0576	620.4
EE-34	7.3472	0.0253	586.8	MM-34	7.2270	0.0502	614.3
EE-35	7.4468	0.1314	570.3	MM-35	7.3564	0.2429	595.7

Table 6: MAFIA calculation: RF-parameters of dipole modes of a 9-cell cavity with beam pipes (EE- and MM-boundary conditions, modes 1 to 35).

mode	f / GHz	R/Q / Ω/cm^2	G_1 /Ω	mode	f / GHz	R/Q / Ω/cm^2	G_1 /Ω
EE-36	7.5430	0.1727	541.4	MM-36	7.4729	0.0291	567.3
EE-37	7.6205	**2.4877**	503.7	MM-37	7.5721	**1.7568**	533.2
EE-38	7.6707	**28.3720**	470.3	MM-38	7.6506	**14.3262**	494.1
EE-39	8.0342	**4.1476**	661.8	MM-39	7.7447	0.0018	599.7
EE-40	8.0342	**2.2097**	661.7	MM-40	7.7470	**18.6850**	585.5
EE-41	8.5040	0.0004	453.5	MM-41	8.3724	0.9746	800.5
EE-42	8.5306	0.0000	464.4	MM-42	8.3724	0.9150	800.5
EE-43	8.5757	0.0043	483.9	MM-43	8.5040	0.0003	453.5
EE-44	8.6386	0.0015	512.5	MM-44	8.5306	0.0000	464.4
EE-45	8.6983	**1.1211**	607.3	MM-45	8.5758	0.0130	484.4
EE-46	8.7121	0.0607	719.8	MM-46	8.6399	0.0074	515.6
EE-47	8.7402	**4.2717**	683.2	MM-47	8.7211	0.5346	558.5
EE-48	8.8270	**5.8193**	668.1	MM-48	8.8117	**5.6496**	611.2
EE-49	8.9185	**5.0744**	721.7	MM-49	8.8977	**9.1801**	670.6
EE-50	9.0017	0.6306	780.2	MM-50	8.9633	0.8384	714.4
EE-51	9.0078	**3.5943**	785.1	MM-51	8.9823	**1.7588**	740.1
EE-52	9.0594	0.0023	1093.6	MM-52	9.0594	0.0007	1093.6
EE-53	9.0602	0.0473	1093.4	MM-53	9.0601	0.0478	1093.2
EE-54	9.0617	0.0604	1096.3	MM-54	9.0617	0.0165	1095.5
EE-55	9.0651	**1.8834**	1110.9	MM-55	9.0648	**1.6172**	1107.4
EE-56	9.0730	**3.3825**	1163.5	MM-56	9.0717	**4.0602**	1148.1
EE-57	9.0945	**1.3124**	1318.1	MM-57	9.0889	**1.8208**	1253.3
EE-58	9.1512	**1.0330**	773.4	MM-58	9.1225	0.0158	1225.9
EE-59	9.1527	0.1031	695.0	MM-59	9.1309	0.1229	1302.2
EE-60	9.1582	**3.1207**	825.0	MM-60	9.1629	0.4827	1044.5
EE-61	9.1607	**3.6345**	974.2	MM-61	9.1641	**2.0427**	1064.5
EE-62	9.2563	**1.2696**	644.0	MM-62	9.1972	0.0006	724.2
EE-63	9.2564	**2.1718**	644.0	MM-63	9.1972	0.0386	724.9
EE-64	9.4064	0.9913	795.3	MM-64	9.3541	0.8037	722.2
EE-65	9.4070	**1.4051**	796.1	MM-65	9.3541	0.0186	722.1
EE-66	9.5152	**4.2015**	752.0	MM-66	9.5899	0.2501	738.2
EE-67	9.5154	0.3551	753.4	MM-67	9.5901	0.0439	738.1
EE-68	9.6867	0.0179	641.4	MM-68	9.6867	0.0000	643.8
EE-69	9.6956	0.1873	640.8	MM-69	9.6986	0.0277	646.2
EE-70	9.7111	0.1572	641.7	MM-70	9.7193	0.0077	647.3

Table 7: MAFIA calculation: RF-parameters of dipole modes of a 9-cell cavity with beam pipes (EE- and MM-boundary conditions, modes 35 to 70).

The boundary conditions at the end of the beam pipe impose a field distribution which is equivalent to a periodic chain of 9-cell cavities which the corresponding symmetry. The influence of the boundary is clearly visible in Fig. 13. But there are also quasi trapped modes which do not depend strongly on the boundary conditions. The electric field of three modes with R/Q above $1\,\Omega/\mathrm{cm}^2$ which are nearly trapped are shown in Fig. 18 to 20. The radial and the longitudinal components of the electric field of mode EE-55 are shown in Fig. 21 and 22. There is a non-vanishing radial component of the electric field in the beam pipe. Therefore the mode is not totally trapped.

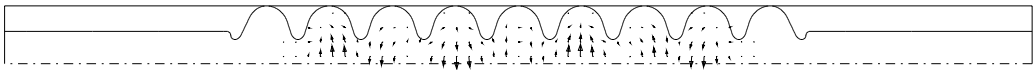

Figure 18: Electric field of the dipole mode EE-55 (MAFIA calculation).

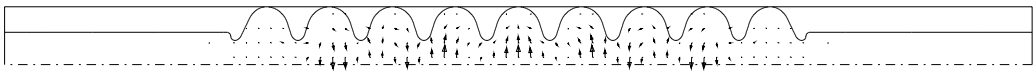

Figure 19: Electric field of the dipole mode EE-56 (MAFIA calculation).

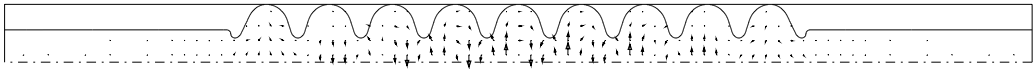

Figure 20: Electric field of the dipole mode EE-57 (MAFIA calculation).

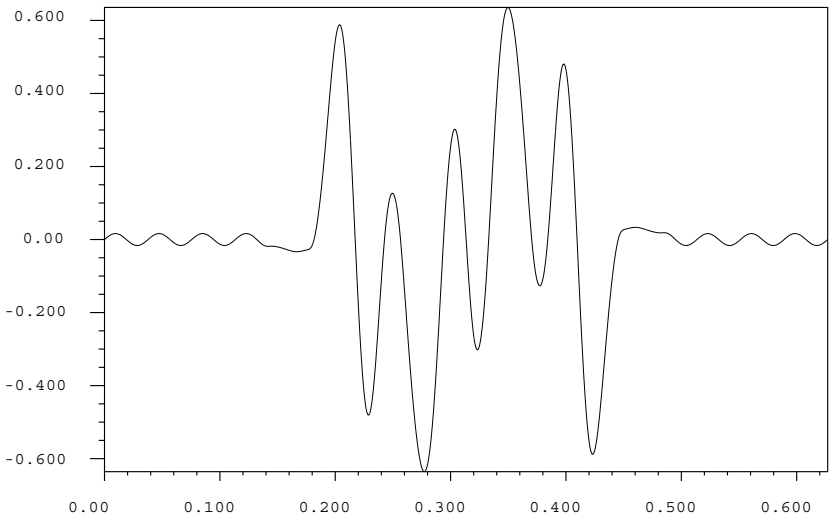

Figure 21: Radial component of the electric field of the dipole mode EE-55 (MAFIA calculation)

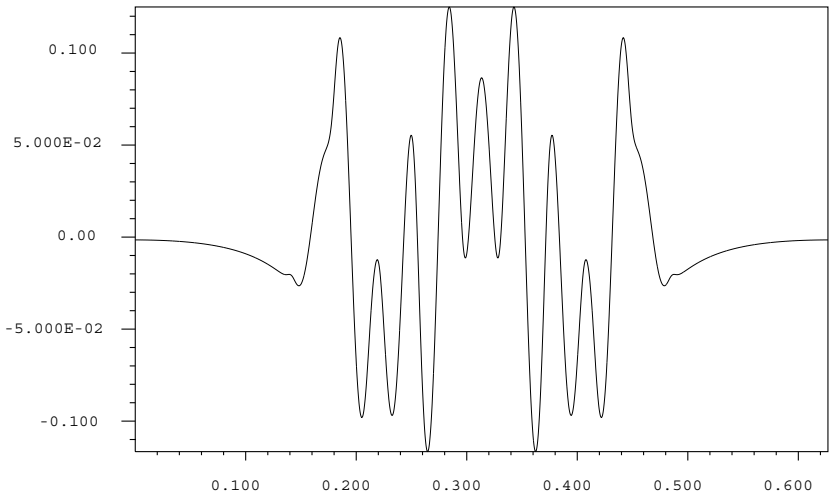

Figure 22: Longitudinal component of the electric field of the dipole mode EE-55 (MAFIA calculation).

All previously obtained results from the MAFIA code have been checked against a special 2-D version of the MWS-code[1] [8]. Due to an improved representation of the cavity geometry within the MWS-code we believe that the result for the mode frequencies from the MWS-code are more accurate than the results from the MAFIA-code. However the relative deviation of the MWS results from the MAFIA results has been found to be less than 0.1 %. The relative difference $(f_{\mathrm{MWS}} - f_{\mathrm{MAFIA}})/f_{\mathrm{MAFIA}}$ is plotted in Fig. 23 versus the frequency f_{MAFIA} of the dipole modes which have been considered. A large relative deviation is found for the modes below the cut-off frequencies of the beam pipe and for the quasi-trapped modes at about 9 GHz. A complete list of results for the frequency and the R/Q is compiled in Tables 8 and 9 for 70 modes with electric (EE) boundary conditions and in Tables 10 and 11 for 70 modes with magnetic (MM) boundary conditions.

The results for R/Q, calculated with MAFIA and MWS, are shown in Fig. 24 for electric boundary conditions and in Fig. 25 for magnetic boundary conditions. The agreement between the codes is good for the first 15 modes. But the MWS-code results for R/Q for modes with higher number (frequencies above 5.3 GHz) differ significantly from the MAFIA results. The ratio $(R/Q)_{\mathrm{MWS}} \,/\, (R/Q)_{\mathrm{MAFIA}}$ is plotted in Fig. 26 versus $(R/Q)_{\mathrm{MAFIA}}$. For all modes with a $(R/Q)_{\mathrm{MAFIA}}$ above $1\,\Omega/\mathrm{cm}^2$ the corresponding values obtained from the MWS-code are smaller.

This difference between the codes is probably due to the different mesh used in MAFIA and MWS. An additional test has been performed with the MAFIA-code using two different mesh sizes. All previous calculations have been done with a fine mesh, with a mesh size of 0.2 mm. Some calculations (EE boundary conditions) have been repeated with a five times coarser mesh (1 mm mesh size). The results for R/Q versus the mode frequencies are shown in Fig. 27. The first 10 to 15 modes agree quite well while the R/Q of higher modes can differ by a factor of two between the two MAFIA cal-

[1] **MI**CRO**W**AVE **S**tudio

culations with different mesh size. The ratio of the R/Q from both MAFIA calculations $(R/Q)_{\mathrm{MAFIA\,1\,mm}}$ / $(R/Q)_{\mathrm{MAFIA\,0.2\,mm}}$ is plotted in Fig. 28 versus $(R/Q)_{\mathrm{MAFIA0.2mm}}$. The ratio scatters around the value of one (identical results for both grids). This is different from the previous comparison between MAFIA and MWS (Fig. 26) which shows a systematic effect that almost all R/Q-values calculated with MWS are smaller than the corresponding R/Q-values obtained from the MAFIA calculation. The results from both MAFIA calculations and the MWS calculation are summarized in Fig. 29 using a linear scale for R/Q. If the MAFIA results are used for tracking calculation to study the beam dynamics in the TTF linac the effect due to dipole modes may be overestimated for all dipole modes above 5 GHz.

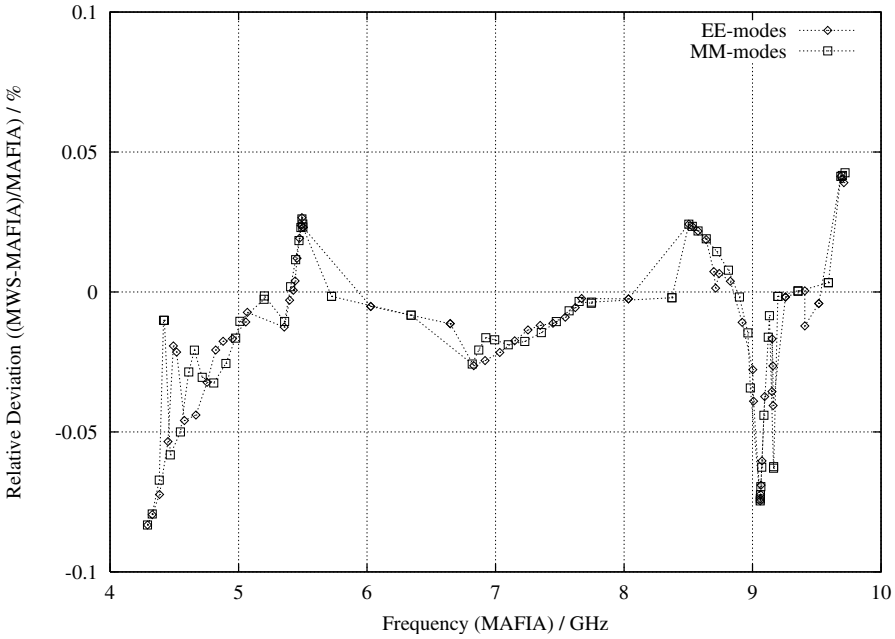

Figure 23: Relative difference of the dipole mode frequencies from MAFIA and MWS calculations in percent versus the frequency from the MAFIA calculation. The result from the MAFIA calculation is used as an reference. Modes with electric (EE) and magnetic (MM) boundary conditions are considered.

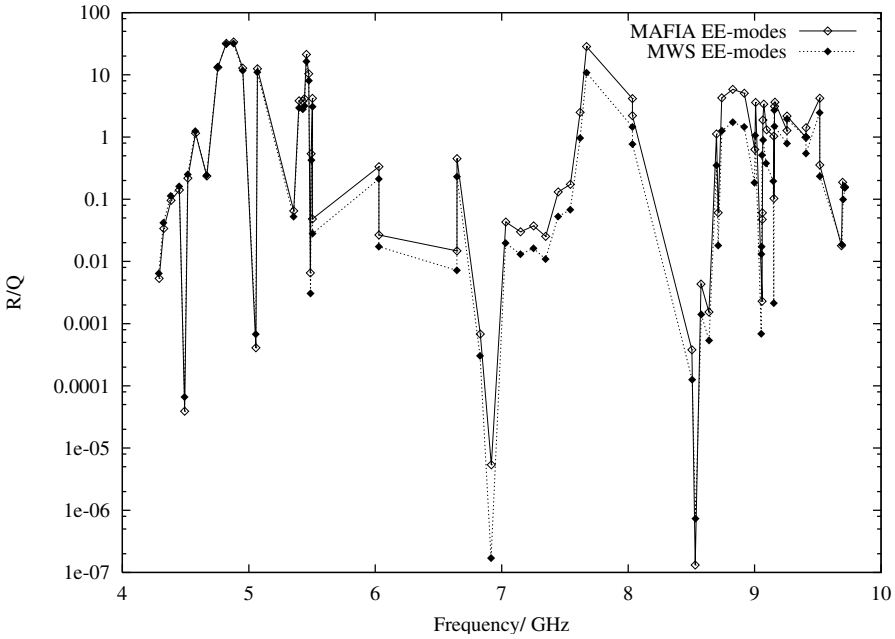

Figure 24: R/Q versus the mode frequency. The results from the MAFIA and MWS calculations are shown for modes with electric (EE) boundary conditions.

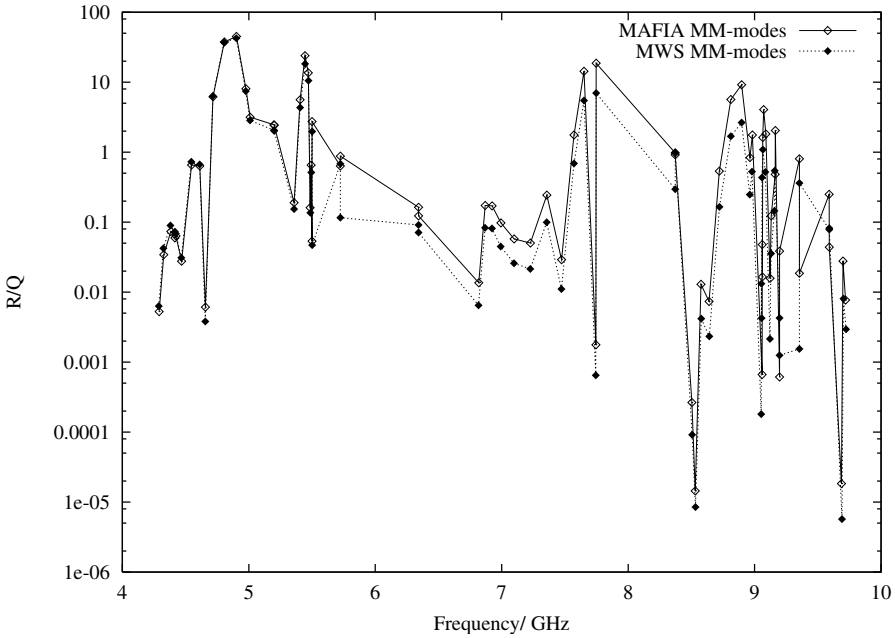

Figure 25: R/Q versus the mode frequency. The results from the MAFIA and MWS calculations are shown for modes with magnetic (MM) boundary conditions.

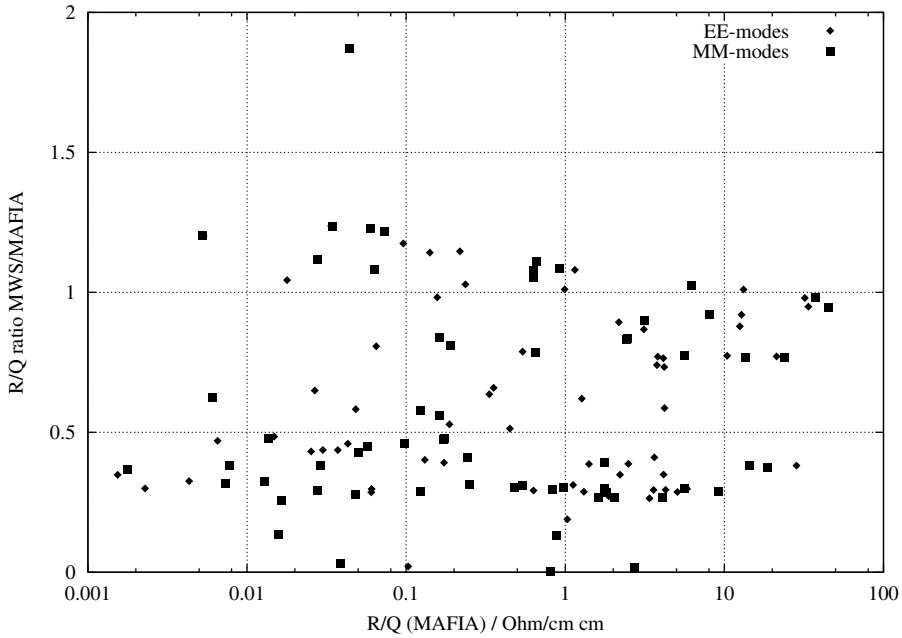

Figure 26: Ratio of the MWS results for R/Q to the MAFIA results for R/Q versus the value R/Q of the MAFIA results. Modes with electric (EE) and magnetic (MM) boundary conditions are considered.

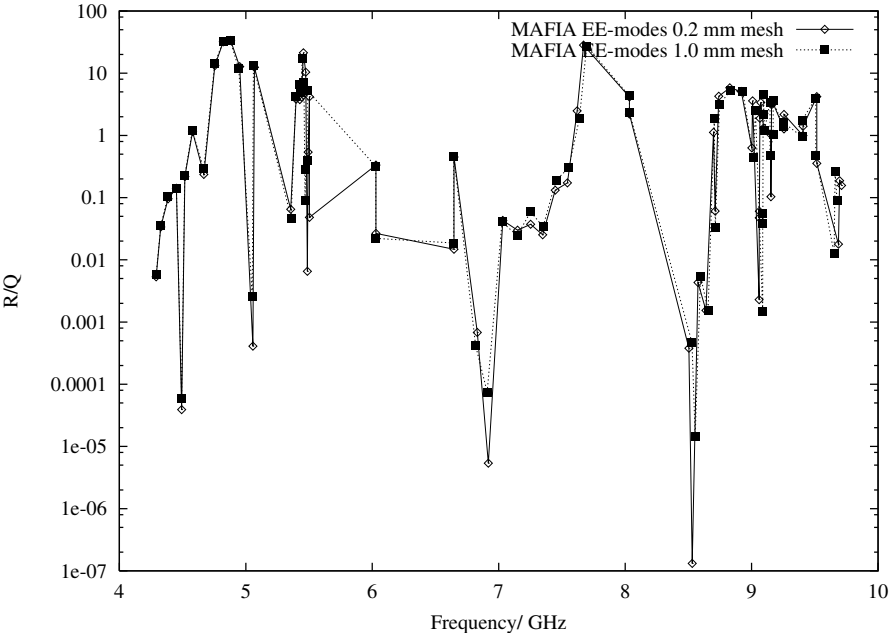

Figure 27: R/Q versus the mode frequency. The results from MAFIA calculations with different mesh size are shown for modes with magnetic (EE) boundary conditions.

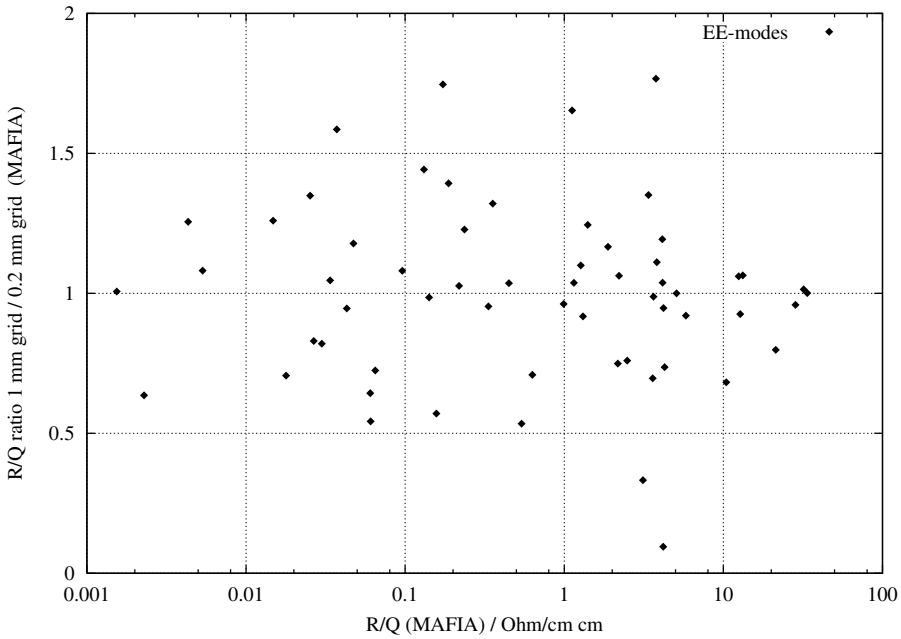

Figure 28: Ratio of the MAFIA results for R/Q with different mesh size (1 mm / 0.2 mm) versus the value R/Q of the MAFIA results (0.2 mm mesh). Only modes with electric (EE) boundary conditions are considered.

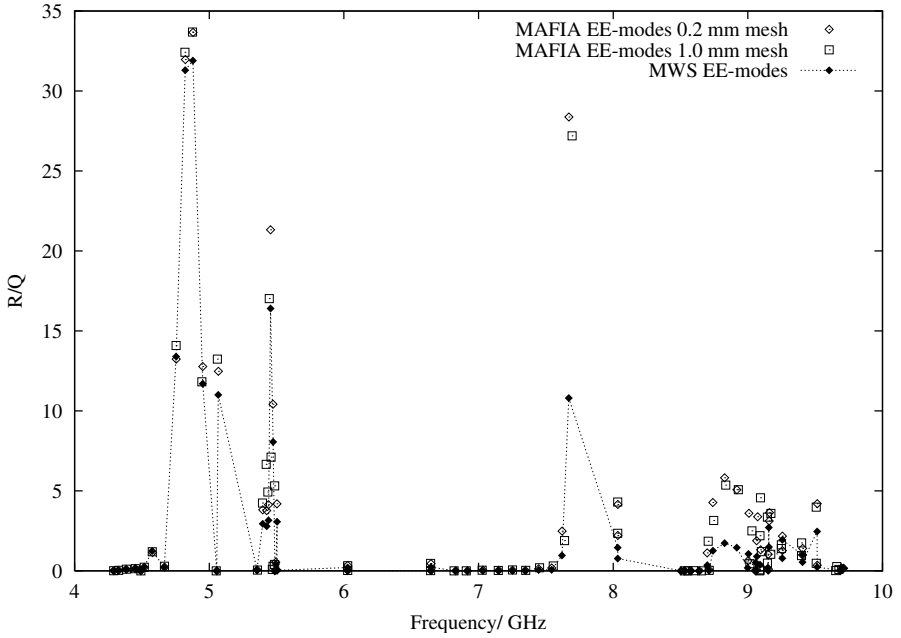

Figure 29: R/Q versus the mode frequency. The results from MAFIA calculations with different mesh size and the results from a MWS calculation are shown for modes with magnetic (EE) boundary conditions.

	MAFIA		MWS	
mode	f / GHz	R/Q / Ω/cm^2	f / GHz	R/Q / Ω/cm^2
EE- 1	4.2911	0.0053	4.2875	0.0064
EE- 2	4.3278	0.0338	4.3244	0.0418
EE- 3	4.3850	0.0959	4.3818	0.1126
EE- 4	4.4512	0.1413	4.4488	0.1613
EE- 5	4.4922	0.0000	4.4914	0.0001
EE- 6	4.5179	0.2182	4.5169	0.2501
EE- 7	4.5783	1.1490	4.5762	1.2409
EE- 8	4.6680	0.2361	4.6660	0.2428
EE- 9	4.7552	13.2378	4.7536	13.3724
EE-10	4.8220	31.9650	4.8210	31.3196
EE-11	4.8797	33.6595	4.8789	31.9403
EE-12	4.9522	12.7711	4.9513	11.7488
EE-13	5.0561	0.0004	5.0555	0.0007
EE-14	5.0678	12.4796	5.0674	10.9660
EE-15	5.3551	0.0648	5.3544	0.0523
EE-16	5.3976	3.8163	5.3974	2.9397
EE-17	5.4267	3.7699	5.4267	2.7893
EE-18	5.4402	4.1318	5.4404	3.1585
EE-19	5.4551	21.3217	5.4557	16.4368
EE-20	5.4737	10.4197	5.4747	8.0581
EE-21	5.4867	0.0065	5.4880	0.0031
EE-22	5.4933	0.5394	5.4948	0.4251
EE-23	5.5027	4.1888	5.5040	3.0708
EE-24	5.5027	0.0482	5.5040	0.0281
EE-25	6.0286	0.3334	6.0283	0.2120
EE-26	6.0286	0.0266	6.0283	0.0173
EE-27	6.6464	0.0148	6.6457	0.0072
EE-28	6.6467	0.4492	6.6460	0.2306
EE-29	6.8306	0.0007	6.8288	0.0003
EE-30	6.9180	0.0000	6.9163	0.0000
EE-31	7.0324	0.0430	7.0309	0.0197
EE-32	7.1491	0.0300	7.1479	0.0131
EE-33	7.2519	0.0372	7.2509	0.0162
EE-34	7.3472	0.0253	7.3463	0.0109
EE-35	7.4468	0.1314	7.4459	0.0527

Table 8: Comparison between the results from the MAFIA and MWS calculations.

	MAFIA		MWS	
mode	f / GHz	R/Q / Ω/cm^2	f / GHz	R/Q / Ω/cm^2
EE-36	7.5430	0.1727	7.5423	0.0677
EE-37	7.6205	2.4877	7.6200	0.9633
EE-38	7.6707	28.3720	7.6705	10.8146
EE-39	8.0342	4.1476	8.0340	1.4474
EE-40	8.0342	2.2097	8.0340	0.7696
EE-41	8.5040	0.0004	8.5061	0.0001
EE-42	8.5306	0.0000	8.5326	0.0000
EE-43	8.5757	0.0043	8.5775	0.0014
EE-44	8.6386	0.0015	8.6403	0.0005
EE-45	8.6983	1.1211	8.6989	0.3496
EE-46	8.7121	0.0607	8.7122	0.0180
EE-47	8.7402	4.2717	8.7408	1.2575
EE-48	8.8270	5.8193	8.8273	1.7346
EE-49	8.9185	5.0744	8.9175	1.4549
EE-50	9.0017	0.6306	8.9992	0.1842
EE-51	9.0078	3.5943	9.0043	1.0561
EE-52	9.0594	0.0023	9.0527	0.0007
EE-53	9.0602	0.0473	9.0535	0.0131
EE-54	9.0617	0.0604	9.0552	0.0173
EE-55	9.0651	1.8834	9.0589	0.5111
EE-56	9.0730	3.3825	9.0675	0.8938
EE-57	9.0945	1.3124	9.0911	0.3771
EE-58	9.1512	1.0330	9.1480	0.1952
EE-59	9.1527	0.1031	9.1512	0.0021
EE-60	9.1582	3.1207	9.1558	2.7072
EE-61	9.1607	3.6345	9.1570	1.4916
EE-62	9.2563	1.2696	9.2561	0.7874
EE-63	9.2564	2.1718	9.2562	1.9399
EE-64	9.4064	0.9913	9.4064	1.0018
EE-65	9.4070	1.4051	9.4058	0.5432
EE-66	9.5152	4.2015	9.5148	2.4645
EE-67	9.5154	0.3551	9.5151	0.2340
EE-68	9.6867	0.0179	9.6907	0.0186
EE-69	9.6956	0.1873	9.6995	0.0989
EE-70	9.7111	0.1572	9.7149	0.1544

Table 9: Comparison between the results from the MAFIA and MWS calculations.

	MAFIA		MWS	
mode	f / GHz	R/Q / Ω/cm^2	f / GHz	R/Q / Ω/cm^2
MM- 1	4.2911	0.0053	4.2875	0.0063
MM- 2	4.3277	0.0343	4.3243	0.0423
MM- 3	4.3831	0.0735	4.3801	0.0894
MM- 4	4.4157	0.0596	4.4152	0.0731
MM- 5	4.4232	0.0635	4.4228	0.0687
MM- 6	4.4683	0.0277	4.4657	0.0309
MM- 7	4.5471	0.6554	4.5449	0.7279
MM- 8	4.6120	0.6350	4.6107	0.6683
MM- 9	4.6567	0.0061	4.6557	0.0038
MM-10	4.7169	6.1772	4.7155	6.3196
MM-11	4.8065	37.6291	4.8050	36.8734
MM-12	4.9018	44.9945	4.9005	42.5036
MM-13	4.9773	8.0710	4.9765	7.4357
MM-14	5.0104	3.1643	5.0099	2.8469
MM-15	5.1993	2.4742	5.1991	2.0615
MM-16	5.2012	2.4102	5.2012	2.0075
MM-17	5.3583	0.1900	5.3578	0.1541
MM-18	5.4056	5.6064	5.4057	4.3376
MM-19	5.4444	23.8903	5.4450	18.3209
MM-20	5.4702	13.6416	5.4712	10.4861
MM-21	5.4853	0.1614	5.4866	0.1355
MM-22	5.4929	0.6536	5.4944	0.5137
MM-23	5.5000	0.0536	5.5014	1.9747
MM-24	5.5001	2.7383	5.5013	0.0471
MM-25	5.7236	0.6329	5.7235	0.6816
MM-26	5.7236	0.8758	5.7235	0.1156
MM-27	6.3426	0.1631	6.3421	0.0911
MM-28	6.3426	0.1226	6.3421	0.0711
MM-29	6.8185	0.0136	6.8168	0.0065
MM-30	6.8693	0.1734	6.8678	0.0830
MM-31	6.9238	0.1714	6.9227	0.0812
MM-32	6.9934	0.0975	6.9922	0.0449
MM-33	7.0985	0.0576	7.0972	0.0259
MM-34	7.2270	0.0502	7.2257	0.0214
MM-35	7.3564	0.2429	7.3554	0.0995

Table 10: Comparison between the results from the MAFIA and MWS calculations.

	MAFIA		MWS	
mode	f / GHz	R/Q / Ω/cm^2	f / GHz	R/Q / Ω/cm^2
MM-36	7.4729	0.0291	7.4721	0.0111
MM-37	7.5721	1.7568	7.5715	0.6896
MM-38	7.6506	14.3262	7.6503	5.4751
MM-39	7.7447	0.0018	7.7444	0.0006
MM-40	7.7470	18.6850	7.7467	7.0025
MM-41	8.3724	0.9746	8.3722	0.2950
MM-42	8.3724	0.9150	8.3722	0.9926
MM-43	8.5040	0.0003	8.5061	0.0001
MM-44	8.5306	0.0000	8.5326	0.0000
MM-45	8.5758	0.0130	8.5776	0.0042
MM-46	8.6399	0.0074	8.6415	0.0023
MM-47	8.7211	0.5346	8.7224	0.1652
MM-48	8.8117	5.6496	8.8124	1.6882
MM-49	8.8977	9.1801	8.8975	2.6510
MM-50	8.9633	0.8384	8.9620	0.2478
MM-51	8.9823	1.7588	8.9792	0.5265
MM-52	9.0594	0.0007	9.0527	0.0002
MM-53	9.0601	0.0478	9.0534	0.0132
MM-54	9.0617	0.0165	9.0551	0.0042
MM-55	9.0648	1.6172	9.0585	0.4342
MM-56	9.0717	4.0602	9.0660	1.0916
MM-57	9.0889	1.8208	9.0849	0.5200
MM-58	9.1225	0.0158	9.1210	0.0021
MM-59	9.1309	0.1229	9.1302	0.0356
MM-60	9.1629	0.4827	9.1571	0.1454
MM-61	9.1641	2.0427	9.1584	0.5433
MM-62	9.1972	0.0006	9.1970	0.0043
MM-63	9.1972	0.0386	9.1971	0.0013
MM-64	9.3541	0.8037	9.3542	0.0015
MM-65	9.3541	0.0186	9.3542	0.3617
MM-66	9.5899	0.2501	9.5902	0.0783
MM-67	9.5901	0.0439	9.5905	0.0821
MM-68	9.6867	0.0000	9.6907	0.0000
MM-69	9.6986	0.0277	9.7026	0.0081
MM-70	9.7193	0.0077	9.7234	0.0029

Table 11: Comparison between the results from the MAFIA and MWS calculations.

4 Conclusion

A cavity shape for a third harmonic cavity (3.9 GHz) for the TESLA test facility (phase II) has been designed. The purpose of the cavity is the compensation of nonlinear distortions of the longitudinal phase space due to the cosine-like curvature of the cavity voltage of the 1.3 GHz cavities. The choice of the frequency of 3.9 GHz was motivated mainly by the rf-amplitude required for the compensation and a broad flexibility with respect to a multi-bunch operation of the TESLA test facility. It was not possible to scale the 1.3 GHz TESLA cavity simply by a factor of three since the dimension of the beam pipe would be too small to mount a coaxial input coupler and the HOM-coupler on the beam pipe.

The rf-parameters of the accelerating mode as well as of higher monopole and dipole modes have been calculated with the computer codes FD-FEM, MAFIA and MWS. Extended listings of these modes are provided for beam dynamics studies. Nearly all dipole modes can propagate into the beam pipe with a few exceptions. The first four dipole modes which have a low R/Q are below the cutoff frequency of the beam pipe and there are a few quasi-trapped modes with frequencies of about 9 GHz. Some of these modes have nearly no field in the cavity end-cells. The determination of the external Q-vales was beyond the scope of this paper.

Further studies are required to calculate the longitudinal wakefields of the 3.9 GHz cavity in the time domain since the wakefields add nonlinear distortions to the cavity voltage which can be larger, depending on the bunch length, than the effects due to the cosine-like curvature of the cavity voltage as shown in Ref. [9] for the 1.3 GHz TESLA cavity.

Acknowledgment

We would like to thank M. Lomperski for carefully reading the manuscript and M. Dohlus for helpful discussions.

References

[1] K. Flöttmann, T. Limberg, Ph. Piot, *Generation of ultrashort electron bunches by cancellation of nonlinear distortions in the longitudinal phase space*, TESLA-FEL-2001-06

[2] B. Aune *et al.*, *The superconducting TESLA cavities*, Phys. Rev. ST Accel. Beams**3** (2000) 092001 [physics/0003011].

[3] K.L. Brown, D.C. Carey, Ch. Iselin, F. Rothacker, *TRANSPORT a computer program for designing charged particle beam transport systems*, CERN 80-04, SPS Division, March 1980

[4] T. Weiland, R. Wanzenberg, *Wake fields and impedances*, in: Joint US-CERN part. acc. school, Hilton Head Island, SC, USA, 7 - 14 Nov 1990 / Ed. by M Dienes, M Month and S Turner. - Springer, Berlin, 1992- (Lecture notes in physics ; 400) - pp.39-79

[5] J. Sekutowicz, *2D FEM code with third order approximation for rf cavity computation*, Proc. of the 1994 Int. Linac Conf. (LINAC 94), ed. K. Takata, Y. Yamazaki, K. Nakahara, Aug. 21-26, 1994, Tsukuba, Japan

[6] T. Weiland, *On the numerical solution of Maxwell's Equations and Applications in the Field of Accelerator Physics*, Part. Acc. 15 (1984), 245-292

[7] *MAFIA Release 4 (V4.021)* CST GmbH, Bad Nauheimer Str. 19, 64289 Darmstadt, Germany

[8] *CST MICROWAVE STUDIO* CST GmbH, Bad Nauheimer Str. 19, 64289 Darmstadt, Germany

[9] A. Novokhatski, M. Timm, T. Weiland, *Single Bunch Energy Spread in the TESLA Cryomodule* TESLA-99-16, Sept. 1999